Two-dimensional birefringence imaging in biological tissue by polarization-sensitive optical coherence tomography

Johannes F. de Boer

Laser Center, Academical Medical Center, Meibergdreef 9, 1105 AZ Amsterdam, The Netherlands, and Beckman Laser Institute and Medical Clinic, University of California, Irvine, Irvine, California 92612

Thomas E. Milner

Beckman Laser Institute and Medical Clinic, University of California, Irvine, Irvine, California 92612

Martin J. C. van Gemert

Laser Center, Academical Medical Center, Meibergdreef 9, 1105 AZ Amsterdam, The Netherlands, and Beckman Laser Institute and Medical Clinic, University of California, Irvine, Irvine, California 92612

J. Stuart Nelson

Beckman Laser Institute and Medical Clinic, University of California, Irvine, Irvine, California 92612

Received January 13, 1997

Using a low-coherence Michelson interferometer, we measure two-dimensional images of optical birefringence in bovine tendon as a function of depth. Polarization-sensitive detection of the signal formed by interference of backscattered light from the sample and a mirror in the reference arm give the optical phase delay between light that is propagating along the fast and slow axes of the birefringent tendon. Images showing the change in birefringence in response to laser irradiation are presented. The technique permits rapid noncontact investigation of tissue structural properties through two-dimensional imaging of birefringence. © 1997 Optical Society of America

The demand for noninvasive optical imaging in biological tissue has led to the development of several techniques to circumvent the common problem of scattering in turbid media; such techniques include diffusing-wave spectroscopy,[1] time-gated imaging using snakelike photons,[2] two-photon fluorescence imaging,[3] ultrasonic modulation of diffusing waves,[4,5] and optical coherence tomography[6,7] (OCT).

OCT uses the partial coherence properties of a light source to image structures with high resolution (1–15 μm) in turbid media such as biological tissue. The sample is positioned in one arm (the sample arm) of a two-beam interferometer. Interference fringes are formed when the optical path length of light backscattered from the sample matches that from the reference to within the coherence length of the source light. The optical path length in the reference arm acts as a gate on the detection, selecting only light backscattered from the sample that has traveled the same optical path length. By lateral and longitudinal scanning, two-dimensional (2D) OCT images are constructed that map the amplitude of light backscattered from the sample. Lateral resolution is determined by the spot size of the beam focus of incoming light and the collection aperture; longitudinal resolution is determined by the coherence length of source light.

In this Letter we present a combination of OCT and polarization-sensitive detection[8] to record 2D images of the change in polarization of circularly polarized incoming light backscattered from a turbid birefringent sample. In contrast with conventional OCT, in which the magnitude of backscattered light as a function of depth is imaged, we use the backscattered light to image the magnitude of the sample birefringence as a function of depth. 2D maps of birefringence of biological materials can reveal important structural information that is difficult to resolve with other imaging techniques. Partial loss of birefringence is known to be an early indication of tissue thermal damage[9] (e.g., burns or laser treatments). To demonstrate polarization-sensitive OCT, we present 1-mm-wide by 700-μm-deep images of bovine tendon birefringence before and after pulsed laser irradiation.

Figure 1 shows a schematic of the polarization-sensitive OCT system used in our experiments. Light passes through a Glan–Thompson polarizer to select a pure linear vertical input state and is split into reference and sample arms by a polarization-insensitive beam splitter (reflection and transmission coefficients for linear vertical and horizontal polarization states were 0.5 ± 0.05). Light in the reference arm passes through a zero-order quarter-wave plate (QWP), rotating at $\Theta = 200\pi$ rad/s. Following reflection from a planar mirror and a return pass through the QWP, light in the reference arm has a rotating linear polarization (400π rad/s). For improved signal–noise ratio,[10] a neutral-density filter positioned in the reference arm reduces intensity noise by a factor of 50. Light in the sample arm passes through

0146-9592/97/120934-03$10.00/0

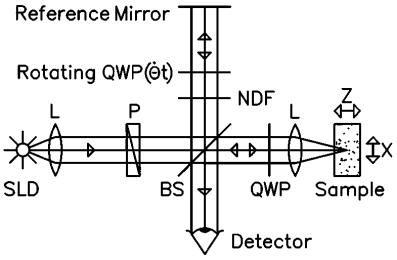

Fig. 1. Schematic of the polarization-sensitive OCT setup. SLD, superluminescent diode, 0.8-mW output power, central wavelength $\lambda_0 = 862$ nm, spectral FWHM $\Delta\lambda = 21$ nm $(= \lambda_0^2 \Omega \sqrt{\ln 2}/\pi c)$; P, polarizer; BS, beam splitter; QWP's, quarter-wave plates; NDF, neutral-density filter; L, lens. 2D images are formed by longitudinal movement of the sample with constant velocity $v = 1$ mm/s (z direction), repeated after each 10-μm lateral displacement (x direction).

a QWP oriented at 45° to the incident vertical polarization to give circularly polarized light. After double passage through a lens and the sample, and propagation through the QWP, light in the sample arm is in an arbitrary (elliptical) polarization state, determined by the sample birefringence.

The intensity of the light incident upon the detector is given by recombination of the light in both arms of the interferometer:

$$\langle I \rangle = \langle I_r \rangle + \langle I_s \rangle + 2\,\mathrm{Re}[\langle \mathbf{\Psi}_r^*(t, z_r) \cdot \mathbf{\Psi}_s(t, z_s) \rangle], \quad (1)$$

where $\mathbf{\Psi}(t, z)$ is the light-amplitude field vector, subscripts r and s denote the reference and the sample arms, respectively, $z_{r,s}$ are the optical path lengths, and the angle brackets denote ensemble averaging. The source spectral density $S(\omega)$ is assumed to be Gaussian $\{\propto \exp[-(\omega - \omega_0)^2/\Omega^2]\}$ with FWHM $= 2\Omega\sqrt{\ln 2}$ rad/s. The evolution of the polarization state in each arm of the interferometer is computed with the Jones matrix formalism, where we neglect optical dispersion in the sample and spectral dependence of the zero-order QWP's over the spectrum of the source. The interference intensity between light in the sample and the reference arms can be separated into horizontal, A_H, and vertical, A_V, components that are proportional to the light-amplitude fields backscattered from the sample:

$$\mathrm{Re}[\langle \mathbf{\Psi}_r^*(t, z_r) \cdot \mathbf{\Psi}_s(t, z_s) \rangle] = A_H + A_V\,,$$

$$A_H \approx \sin(2\dot{\Theta}t)\cos(2k_0\Delta z)\exp[-(\Omega\Delta z/c)^2]\cos(k_0 z\delta)\,,$$

$$A_V \approx \cos(2\dot{\Theta}t)\cos(2k_0\Delta z + 2\alpha) \times \exp[-(\Omega\Delta z/c)^2]\sin(k_0 z\delta)\,, \quad (2)$$

where Δz is the optical path-length difference between the sample and the reference arms of the interferometer. In our system Δz is a function of time and longitudinal velocity of the sample, z is the backscatter depth in the sample, $k_0 = 2\pi/\lambda_0$, c is the speed of light in vacuum, δ is the difference in refractive indices along the fast and the slow axes of the birefringent sample $(n_s - n_f)$, $\dot{\Theta}$ is the rotation speed of the QWP in the reference arm, and α is the angle of the fast optical axis of the birefringent sample with the horizontal. The only approximation in Eqs. (2) is that the product of birefringence and propagation depth in the sample (in the present case $z\delta \leq 2.6$ μm) is much smaller than the width of the coherence envelope $(2c/\Omega = 19$ μm).

Phase-sensitive demodulation of the recorded signal with respect to the angular position of the rotating QWP $(\dot{\Theta}t)$ permits separation of the intensities corresponding to vertically and horizontally polarized light. In addition to the carrier frequency $[\cos(2k_0\Delta z)]$ within the coherence envelope $\{\exp[-(\Omega\Delta z/c)^2]\}$ both signals show an oscillation with a periodicity determined by the product of sample birefringence (δ) and propagation depth (z) that allows for birefringence imaging.

We made scans by moving the sample at constant velocity $v = 1$ mm/s, giving a carrier frequency $\nu = 2v/\lambda_0 = 2.4$ kHz. To form 2D images, we recorded a longitudinal scan after each 10-μm lateral displacement of the sample. The 4-mm-diameter beam, focused upon the sample by a lens ($f = 50.2$ mm), gave a 14-μm beam-waist diameter. In air, the sample arm was matched in length to the reference arm at a position 200 μm past the focal point, leading to a matched length in the beam focus ~400 μm deep in a sample with refractive index $n = 1.4$.[11,12] The detector was ac coupled, and the signal was amplified, high-pass filtered at 1 kHz with 18-dB/octave roll-off, and digitized with 16-bit resolution at 50,000 points per second.

Signal processing consisted of squaring the detected signal and phase-sensitive demodulation with respect to $\dot{\Theta}t$ to separate the horizontal, I_H, and vertical, I_V, components of the backscattered light. Then, within each longitudinal scan, data points were averaged with a Gaussian weight function (FWHM 700 data points) to form one image pixel. The resulting signals give the backscattered horizontal and vertical intensities as a function of depth z with a resolution of 10-μm physical distance, modulated with their respective birefringence-dependent terms:

$$I_H(z) \propto \cos^2(k_0 z\delta), \qquad I_V(z) \propto \sin^2(k_0 z\delta)\,. \quad (3)$$

In Fig. 2a, a birefringence image of fresh bovine tendon is shown. Measurements on 1 cm × 2 cm samples at least 1 cm thick were done within 48 h of sacrifice of the bovine. The banded structure, indicative of birefringence, is clearly visible up to a physical depth of 700 μm. By measuring the optical-versus-physical thickness of a thin slice,[11] we found the average refractive index of the tendon to be $\bar{n} = 1.42 \pm 0.03$. We determined the birefringence by measuring the average distance between the start (zero crossing) of the first and the second yellow bands from the top of the figure over the full width of Fig. 2a (100 lateral scans). The average distance $\bar{z} = 116 \pm 13$ μm corresponds to a full period of the sine squared in relations (3), $k_0\bar{z}\delta = \pi$. The measured birefringence $\delta = 3.7 \pm 0.4 \times 10^{-3}$ of bovine tendon (predominantly type I collagen) is in agreement with reported values of $3.0 \pm 0.6 \times 10^{-3}$ (Ref. 13) and 2.8–3.0×10^{-3}.[14,15] Fitting $\exp(-2z/\gamma)$, between $z = 150 - 600$ μm depth, to the total backscattered intensity in the sample, $I_b(z) \propto I_H(z) + I_V(z)$, averaged over the image in Fig. 2a

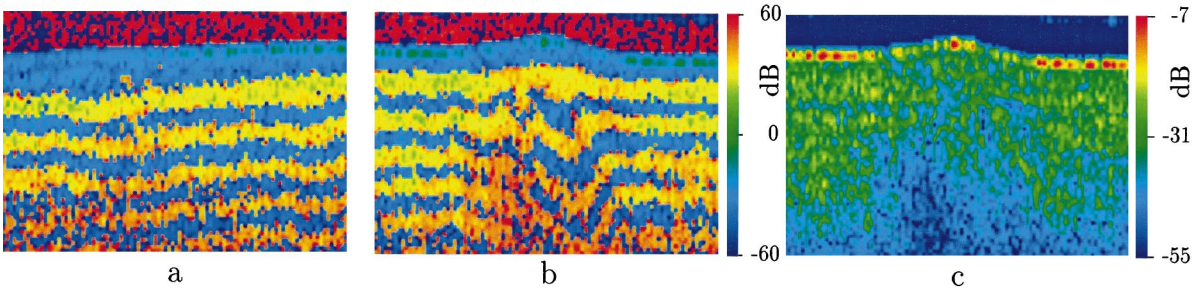

Fig. 2. Images of fresh bovine tendon 1 mm wide by 700 μm deep. Each pixel represents a 10 μm $\times$ 10 μm area. The dynamic range of the system was 48 dB. We generated false color birefringence images a and b by computing $\mathrm{sgn}[I_H(z) - I_V(z)]10 \log|I_H(z) - I_V(z)|$. Noise is represented by deep blue or deep red. The color scale at the right gives the magnitude of signals. The banded structure, indicative of the birefringence, is clearly visible. a, Birefringence image of fresh bovine tendon. b, Birefringence image of bovine tendon following exposure to three consecutive 1-J 150-μs laser pulses ($\lambda = 1.32$ μm) spaced by 10 ms, incident from the upper left at 35° with respect to the surface normal. The beam diameter was 2 mm. Initial surface temperature after laser irradiation was 77 °C, dropping to 61 °C after 0.25 s. c, Total backscattered intensity image of bovine tendon, constructed from the same measurement shown in b to demonstrate differences from the polarization-sensitive image. We generated a false color image by computing $10 \log[I_H(z) + I_V(z)]$. The color scale to the right gives the magnitude of the signals in c.

(100 lateral scans), gives $\gamma \approx 0.2$ mm. Decay of the total backscattered light intensity with depth depends on several factors, among them attenuation of the coherent beam by scattering and the geometry of the collection optics.

In Fig. 2b, a birefringence image of laser-irradiated bovine tendon is presented. The image clearly shows a decrease in the birefringence at the center of the irradiation zone, extending into the tendon over the full depth of the image (700 μm). Further, the direction of incoming laser light (from the upper-left corner, at an angle of 35° with the normal of the surface) is observed. The surface temperature of the tendon was monitored during laser irradiation by IR radiometry. For comparison, Fig. 2c shows an OCT image of the total backscattered intensity $I_b(z)$. Although less backscattered light from the irradiated area can be observed, the polarization-sensitive image (Fig. 2b) reveals important structural information not evident in Fig. 2c.

We have shown that polarization-sensitive optical coherence tomography can reveal structural information on birefringent turbid media such as biological tissue that is not available when polarization-insensitive OCT is used. Polarization-sensitive OCT has the potential to provide guidance regarding optimal dosimetry for thermally mediated laser therapeutic procedures by permitting real-time diagnostics at each irradiated site through detection of changes in birefringence associated with thermal damage and pathological conditions. This would permit a semiquantitative evaluation of the efficacy of laser therapy as a function of incident light dosage.

Research grants from the Biomedical Research Technology Program and the Institute of Arthritis and Musculoskeletal and Skin Diseases of the National Institutes of Health, the Whitaker Foundation (WF 21025), and the Dermatology Foundation are gratefully acknowledged, as is institute support from the U.S. Department of Energy, the National Institutes of Health, and the Beckman Laser Institute Endowment. In addition, J. F. de Boer (JFdB) and M. J. C. van Gemert gratefully acknowledge financial support from the Dutch Technology Foundation (STW, grants AGN 33.2954 and AGN 55.3906) and the Academical Medical Center. JFdB thanks R. Sprik for stimulating discussions.

References

1. A. Yodh and B. Chance, Phys. Today **48**(3), 34 (1995).
2. F. Liu, K. M. Yoo, and R. R. Alfano, Opt. Lett. **19,** 740 (1994).
3. W. Denk, D. W. Piston, and W. W. Webb, in *Handbook of Biological Confocal Microscopy*, J. B. Pawley, ed. (Plenum, New York, 1995), p. 445.
4. L. Wang, S. L. Jacques, and X. Zhao, Opt. Lett. **20,** 629 (1995).
5. M. Kempe, M. Larionov, D. Zaslavsky, and A. Z. Genack, J. Opt. Soc. Am. A **14,** 1151 (1997).
6. D. Huang, E. A. Swanson, C. P. Lin, J. S. Schuman, W. G. Stinson, W. Chang, M. R. Hee, T. Flotte, K. Gregory, C. A. Puliafito, and J. G. Fujimoto, Science **254,** 1178 (1991).
7. A. F. Fercher, J. Biomed. Opt. **1,** 157 (1996).
8. M. R. Hee, D. Huang, E. A. Swanson, and J. G. Fujimoto, J. Opt. Soc. Am. B **9,** 903 (1992).
9. S. Thomsen, Photochem. Photobiol. **53,** 825 (1991).
10. W. V. Sorin and D. M. Baney, IEEE Photon. Technol. Lett. **4,** 1404 (1992).
11. G. J. Tearney, M. E. Brezinski, J. F. Southern, B. E. Bouma, M. R. Hee, and J. G. Fujimoto, Opt. Lett. **20,** 2258 (1995).
12. Z. Chen, T. E. Milner, D. Dave, and J. S. Nelson, Opt. Lett. **22,** 64 (1997).
13. D. J. Maitland and J. T. Walsh, "Quantitative measurements of linear birefringence during the heating of native collagen," Lasers Surg. Med. (to be published); D. J. Maitland, "Dynamic measurements of tissue birefringence: theory and experiments," Ph.D. dissertation (Northwestern University, Evanston, Ill., 1995).
14. E. P. Chang, D. A. Keedy, and C. W. Chien, Biochim. Biophys. Acta **343,** 615 (1974).
15. E. J. Naylor, Q. J. Microsc. Sci. **94,** 83 (1953).